Analysis of the impact of ventilated cavities on the performance of opaque components

Alessandro Prada – Free University of Bolzano, Bolzano, Italy
Marco Baratieri – Free University of Bolzano, Bolzano, Italy
Andrea Gasparella – Free University of Bolzano, Bolzano, Italy

Abstract

The energy performance of buildings depends on the behaviour of the different components under transient conditions, as it happens in particular for the opaque envelope both through its stationary and through its dynamic response to the external solicitations.

Some attempts to improve especially the summer performance of such elements are related to the insertion of air cavities, both still air or naturally ventilated through external openings. In those cases the annual performance evaluation becomes quite difficult, in particular when quasi steady state approaches are considered.

A large number of papers in the literature consider theoretical and experimental analysis of different ventilated components (opaque ventilated walls, roofs, double skin facades, ventilated floors). Daily and annual variations of boundary conditions and their dependence on the specific climatic context further increase the generalization of the results.

Summer improvement of comfort conditions and the reduction of cooling energy needs should be compared with the possible drawbacks during the heating season. This evaluation requires us to consider the entire building envelope and can be generalized only by means of a parametric analysis of the cavities impacts in relation to the composition, geometry, orientation and climatic context both of the cavities and of the building envelope.

In the present paper a thermal and fluid-dynamic analysis of ventilated air cavities is performed under different flow patterns and external conditions. The aim is to analyse the impact on the energy performance of the opaque building components. The values calculated by means of the enhanced model are compared with the predictions obtained with the reference standards.

1. Introduction

Heat transfer modelling of building envelope components with a ventilated air cavity requires the knowledge of the air change rates.

The air motion inside the ventilation channel is closely related to cavity shape, weather conditions (i.e. wind velocity, solar irradiation, air pressure and dry bulb temperature) and to the heat flux transmitted through the envelope. Therefore, to correctly model the wall behaviour, a coupled thermo-fluid dynamic analysis is needed.

In the literature, a large number of papers deal with the problem of modelling the effects of a ventilated air cavity on the summer heat transfer through the envelope (e.g. Ciampi et al., 1998, Ciampi et al., 2003 and Gagliano et al. 2012). Further, since there are few experimental measurements of air velocity in ventilation channels (e.g. Susanti et al., 2008 and Falk et al., 2012), few of these models are validated against experimental data. For this reason, several authors in the past investigated the role of the choice of CFD models and computation domain in the reliability of CFD predictions coupled with heat transfer solutions (e.g. Gan 2010, Nore et al., 2010 and Pasut et al. 2012).

However, in view of the reduction of cooling loads, ventilated air cavities present some drawbacks in winter months. In fact, in cold and humid locations some problems related to moisture infiltration in the opaque components can often occur. Consequently, a high ventilation rate is often required in order to dispose of the excess moisture in the wall. On the other hand, an increase in the heat transmission could be caused by the high air velocity in the cavity. Despite these considerations,

the winter performance of a ventilated wall has been barely investigated up until now.
Therefore, this paper focuses on the investigation of the winter performances of ventilated walls evaluated by means of a thermal-fluid dynamic analysis. In particular the CFD model is used to describe the turbulent air flow rate in the vented cavity caused by a buoyancy effect.
Starting from the heat fluxes calculated by means of the enhanced model, the average surface thermal resistance is then computed. This data, applied in the simple quasi steady state approaches, is then compared with the reference values proposed by the standard EN ISO 6946.

2. Test cases

Since this work aims to investigate the heat exchanges through the wall when ventilated channels are present, numerical simulations with several variants of the cavity are adopted. In particular, the different conditions aim to take into account the influence factors of the heat transfer mechanisms and of the boundary conditions. Two different wall typologies are used with the purpose of analysing both insulated (i.e. Case I) and not insulated (i.e. Case U) constructions (Figure 1). In fact, since in insulated walls the inner surface of the cavity could have lower temperature, the driving factor behind the ventilation flow is greatly reduced.

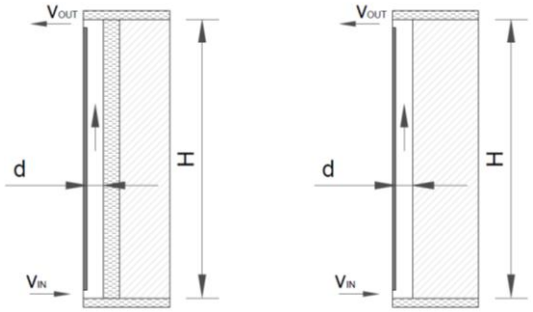

Fig. 1 – Test cases used in the analysis (case I on the left and case U on the right)

Therefore, in the test cases, particular attention is paid to the choice of the characteristics of the wall internal layer. In particular, the thermo-physical properties, used for steady state analysis, which are adopted in this work are shown in Table 1.

Material	**Thickness [*m*]**	**Conductivity [W M^{-1} K^{-1}]**
Concrete Cover	0.02	0.90
EPS insulation	0.05	0.036
Brick block (case I)	0.25	0.34
Brick block (case U)	0.30	0.34

Table 1 – Material property of the solid layer

In addition to the two types just described, the cases analysed are expanded by varying certain parameters. For both cases, the external air temperatures, the emissivity of the cavity inner surface and the shape ratio of the cavity are changed with the purpose of investigating the extent to which each parameter affects the air motion in the channel and, consequently, the heat transfer. The parameter values adopted in the various configurations are reported in Table 2

Variable	**Levels**
T_{ext} [°C]	-10, -5, 0, 5, 10, 15
e_2 [-]	0.1, 0.9
H [m]	3, 6
d [cm]	0.6, 0.10, 0.15

Table 2 – Cavity configuration parameters

The outdoor wind hardly influences the ventilation flow in the cavity. However, the study of the inlet velocity caused by wind forces is strictly connected with site characteristics. For this reason, in this work only the stack effect is investigated by assuming no wind external forces.

3. Simulation model

3.1 Governing equations

In order to model the behaviour of the turbulent system with a low computational cost, the Reynolds-averaged Navier Stokes (RANS) equations are used. Adopting the weakly

compressible hypothesis (i.e. compressibility is taken into account only in continuity equation) and the Newtonian behaviour of the fluid, the system of solved partial differential equations becomes:

Conservation of fluid mass

$$\frac{\partial \rho}{\partial t} + \nabla \cdot (\rho u) = 0 \quad (1)$$

Momentum equation with the eddie closure relation

$$\rho\left(\frac{\partial u}{\partial t} + u \cdot \nabla u\right) = \nabla \cdot \left[-pI + (\eta + \eta_T)\left(\nabla u + (\nabla u)^T - \frac{2}{3}(\nabla \cdot u)I\right) - \frac{2}{3}\rho k I\right] + F \quad (2)$$

Heat equation for solid domain

$$\rho c_p \frac{\partial T}{\partial t} + \nabla \cdot (-\lambda \nabla T) = 0 \quad (3)$$

Heat equation for fluid domain

$$\rho c_p \frac{\partial T}{\partial t} + \nabla \cdot (-(\lambda + \lambda_T)\nabla T) = -\rho c_p u \nabla T \quad (4)$$

Transport equation of the turbulent kinetic energy

$$\rho\left(\frac{\partial k}{\partial t} + u \cdot \nabla k\right) = \nabla \cdot [(\eta + \eta_T)\nabla k] + \frac{1}{2}\eta_T(\nabla u + (\nabla u)^T)^2 - \rho\varepsilon \quad (5)$$

Transport equation of the turbulent energy dissipation rate

$$\rho\left(\frac{\partial \varepsilon}{\partial t} + u \cdot \nabla \varepsilon\right) = -\rho C_{\varepsilon 2}\frac{\varepsilon^2}{k}\nabla \cdot \left[\left(\eta + \frac{\eta_T}{1.3}\right)\nabla \varepsilon\right] + \frac{1}{2}C_{\varepsilon 1}\frac{\varepsilon}{k}\eta_T(\nabla u + (\nabla u)^T)^2 \quad (6)$$

where η_T is the eddy viscosity computed as:

$$\eta_T = \rho C_\eta \frac{\varepsilon^2}{k} \quad (7)$$

3.2 Numerical discretization

The first step in the problem solution is the numerical discretization of the problem of air motion and of heat transfer through the ventilated channel. Figure 2 visualizes the spatial discretization by means of triangular finite element of the upper part of the 2D model reported in Figure 1.

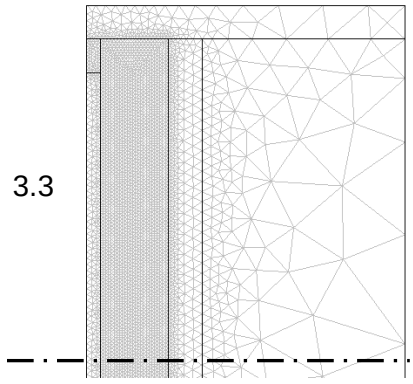

Fig. 2 – Typical mesh discretization adopted.

Note that, with the purpose of increasing the simulation accuracy and at the same time limiting the computational cost, the domain is discretized with a greater thickening in the zone of the convective heat exchange between the air flow and the wall surface.

Since the momentum equations (eq. 2) are nonlinear, the solution of the coupled heat and fluid dynamic problem becomes unstable if the Galerkin finite element method is adopted for the spatial discretization of the domain (Hauke, 2002). Consequently, in all the turbulent simulations herein reported an artificial diffusion is introduced. The diffusion is required in order to ensure the numerical convergence of the problem solution. However, the artificial diffusion parameter is kept to as low a value as possible while still getting a converged simulation.

3.4 Boundary conditions

In order to univocally solve the problem, boundary conditions are required. For instance, for the RANS equations the pressure at the inlet and outlet sections is imposed (Table 3). In addition to the pressure condition, at the outlet section also the condition of vanishing viscous stress along the boundary is imposed.

Boundary	**RANS**	**Heat trans.**
Inlet	$p = p_{atm}$	$T = T_{ext}$
Outlet	$p = p_{atm} - \rho g H$	$-\hat{n} \cdot (-\lambda \nabla T) = 0$
Wall	$-\hat{n} \cdot u = 0$ Log. wall function	Log. wall function

Table 3 – RANS e heat transfer BC for fluid domain

For the other boundaries, the turbulence close to the solid wall is very different from isotropic free-stream turbulence and this should be taken into account. In this work the adopted approach is the so-called wall functions. In this method, an empirical logarithmic relation between the value of velocity and wall friction replaces the thin boundary layer close to the wall. Then, for the heat transfer problem, the inlet temperature and the convective BC are imposed respectively at the inlet and outlet sections. Similarly, a series of boundary

conditions are imposed also for the solid domain (Table 4).

Boundary	Heat transfer
Internal surface	$-\hat{n}\cdot(-\lambda\nabla T)=h_{int}(T-20°C)$
External surface	$-\hat{n}\cdot(-\lambda\nabla T)=h_{ext}(T-T_{ext})$
Cut-off	$-\hat{n}\cdot(-\lambda\nabla T)=0$

Table 4 – Heat transfer BC for solid domain

In particular, while for the internal and external surfaces the Robin-Newton condition is used, for the cut off plane (i.e. the bottom and upper surfaces) the adiabatic conditions are adopted.

4. Results

As a first step in the result analysis the velocity field is herein presented. Figure 3 shows the velocity field and the streamline obtained at the inlet and outlet sections for the case I. The figure clearly shows the stagnant region in the inlet portion of the cavity that produces an increasing velocity on the other side of the ventilation channel. Similarly, due to the narrowing, the air speed increases at the cavity outlet.

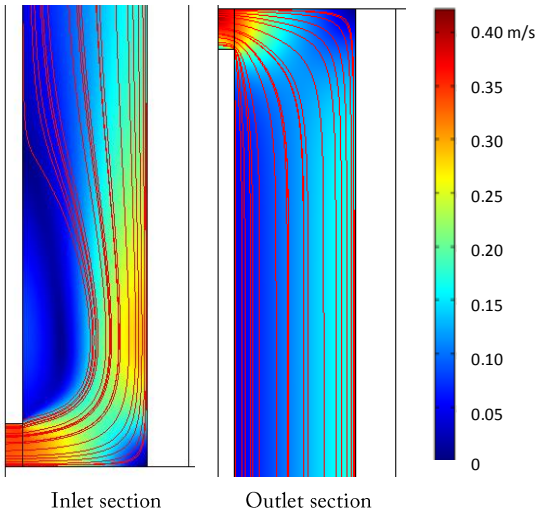

Fig. 3 – Velocity field in the channel at inlet and outlet (case I with d=15 cm, e2=0.1 and Text=0°C)

Besides, it is interesting to note that in areas far from the edge regions, the air speed induced by the stack effect settles around 0.15 - 0.20 [m s^{-1}].

In the following paragraphs the results of the comparisons between the surface thermal resistances, provided by the annex A of the standard EN ISO 6946, and the values obtained from the post-processing of thermo-fluid dynamics simulations are reported. In particular, starting from the heat flux density computed by means of the finite element method, the surface thermal resistance is computed by means of equation 8.

$$R_{se}=\frac{T_i-T_e}{\phi}-\sum_j {s_j}/{\lambda_j}-R_{si} \qquad (8)$$

Using this relation for each configuration an equivalent average thermal resistance of the vented cavity are computed. The values obtained are reported in Table 5

Besides, a study of the influence of cavity parameters on the surface thermal resistance is herein presented. In these sections, the way in which the boundary configurations affect the reduction of the surface resistance is analysed. In particular, the parameter investigated are the cavity height, the emissivity of the cavity inner surface, the insulation level of the wall behind the ventilation channel and the inlet air temperature.

4.1 Effect of cavity thickness

The increasing of cavity thickness induces an adjustment in the air motion characteristics. In fact, air passes from a laminar flow to a transition regime or turbulent motion. Consequently, it also increases the heat transfer between the fluid and the inner cavity surface.

Figure 4 and Figure 5 show respectively the trends of surface thermal resistance as a function of cavity thickness for high and low emissivity of the inner surface. The points names represent the parameters used in the configuration adopted, i.e. insulated (I) or uninsulated (U) wall combined with either 3 or 6 metres of cavity height. Both figures show increasing surface thermal resistance for high cavity height. In fact, the higher the cavity height the lower the influence of inlet and outlet turbulent region. Further, for long ventilation channels, in the top region the temperature difference and, consequently, the convective heat transfer decrease.

		$e_2 = 0.1$				$e_2 = 0.9$			
	Te [°C]	U3	I3	U6	I6	U3	I3	U6	I6
d = 6 cm	-10	0.367	0.374	0.400	0.428	0.199	0.186	0.210	0.211
	-5	0.375	0.383	0.411	0.439	0.198	0.185	0.208	0.209
	0	0.386	0.395	0.424	0.454	0.197	0.184	0.208	0.207
	5	0.401	0.412	0.439	0.472	0.197	0.184	0.208	0.207
	10	0.428	0.439	0.469	0.504	0.199	0.185	0.210	0.210
	15	0.480	0.492	0.534	0.573	0.206	0.185	0.209	0.209
d = 10 cm	-10	0.341	0.346	0.365	0.388	0.193	0.180	0.202	0.203
	-5	0.348	0.354	0.374	0.399	0.192	0.179	0.201	0.201
	0	0.358	0.365	0.386	0.413	0.191	0.178	0.201	0.201
	5	0.373	0.381	0.401	0.429	0.191	0.179	0.201	0.201
	10	0.398	0.406	0.427	0.457	0.195	0.182	0.205	0.205
	15	0.453	0.462	0.486	0.520	0.203	0.189	0.213	0.213
d = 15 cm	-10	0.327	0.329	0.344	0.365	0.188	0.176	0.196	0.197
	-5	0.333	0.337	0.352	0.374	0.187	0.175	0.197	0.197
	0	0.342	0.349	0.363	0.386	0.187	0.176	0.195	0.195
	5	0.355	0.364	0.378	0.402	0.187	0.176	0.196	0.195
	10	0.377	0.389	0.403	0.429	0.191	0.180	0.196	0.195
	15	0.423	0.441	0.459	0.489	0.200	0.187	0.204	0.203

Table 5 – Surface thermal resistance obtained by thermo fluid-dynamic analysis

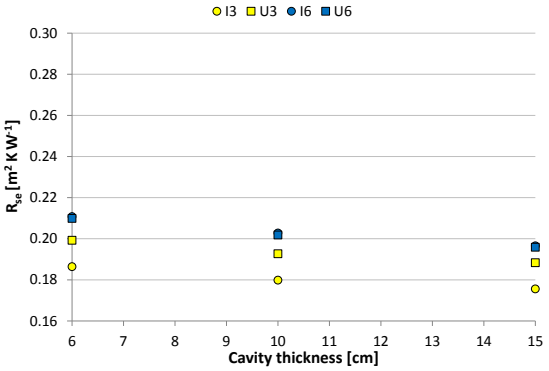

Fig. 4 – Surface resistance as a function of cavity thickness (e2 = 0.9 and Te = -10°C)

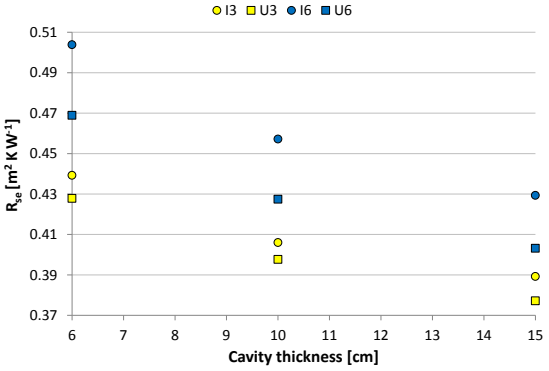

Fig. 5 – Surface resistance as a function of cavity thickness (e2 = 0.1 and Te = -10°C)

Similarly the surface equivalent thermal resistance of the cavity decreases for high cavity thickness, as is shown both in figure 4 and in figure 5. Also in this case, the reduction of the average surface equivalent resistance is caused by the increasing vorticity of the air motion.

It should be remarked that the values plotted in Figure 4 and in Figure 5 are in quite a good agreement with the surface resistance obtained by means of the calculation procedure provide by the annex A of EN ISO 6946. In fact, the standard values using an outside temperature of -10 °C are 0.170 [m² K W^{-1}] and 0.344 [m² K W^{-1}], respectively adopting an emissivity of 0.9 and 0.1 for the inner cavity surface.

Furthermore, Figure 4 points out the different behaviour between 3 and 6 metres of cavity height. In fact, while no appreciable differences are noted between cases U6 and I6, case I3 shows lower equivalent resistance with respect to case U3. These results suggest that for tall cavities the pressure difference between the outlet and inlet section is the primary cause of the air motion. Therefore, no appreciable variations in the mean air speed are noted even if the surface temperature changes between cases I and U. On the contrary, in short cavities the pressure gradient is limited and

the air motion is mainly induced by the variation of air specific mass. In fact, Figure 4 highlights lower resistance for case I3 where the cavity inner surface temperature is higher. This behaviour is not found, however, when the cavity inner surface has low emissivity (Figure 5). In these configurations, the component of radiative thermal resistance increases and, therefore, the behaviour is closely related to the shape aspect ratio. In addition, despite the high surface temperature, the increase radiative thermal resistance ensure a high thermal resistance in the cases I with respect to uninsulated cases.

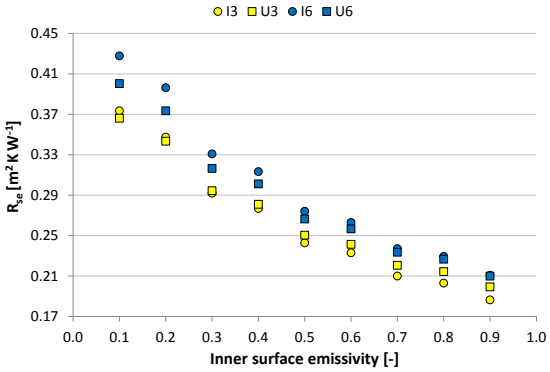

Fig. 6 – Surface resistance as a function of inner surface emissivity (d = 6 cm, Te = -10°C)

These preliminary results therefore show two different behaviours of the vented cavity that are influenced by the surface characteristics and by boundary conditions. These variations are even more visible by analysing the equivalent resistance plotted as a function of the inner surface emissivity of the cavity (Figure 6). In fact low surface emissivity ensures high radiative thermal resistance and higher temperature of the inner surface of the vented channel. However, these high temperatures help the air motion inside the cavity and, consequently, they reduce the convective thermal resistance.

Therefore for 3 metre cavities when the inner surface has emissivity lower than 0.3 despite the higher surface temperature of case I3 that favours the air motion, the low emissivity value coupled with the reduced difference between the fourth powers of the surface temperatures greatly reduce the heat exchange by radiation. Consequently case I3 shows a value of total equivalent thermal resistance higher than case U3.

On the other hand, if the inner surface emissivity is greater than 0.3, the increase of radiative heat transfer prevails on the reduction of the convective exchange. For this reason, the case U3 shows a total equivalent thermal resistance higher than case I3.

The threshold for the transition between the first and the second behaviour of the ventilation channel will of course depend on the characteristics of the motion and therefore on the cavity shape. For example in Figure 6 it seems that, for the 6 metre length, the transition occurs for emissivity of 0.9. Hence the increasing of the cavity height induces a greater emissivity threshold. In fact, as already pointed out and better described for the velocity profiles (Figure 7), the lower inner surface emissivity favours the motion of the fluid and therefore the convective heat transfer.

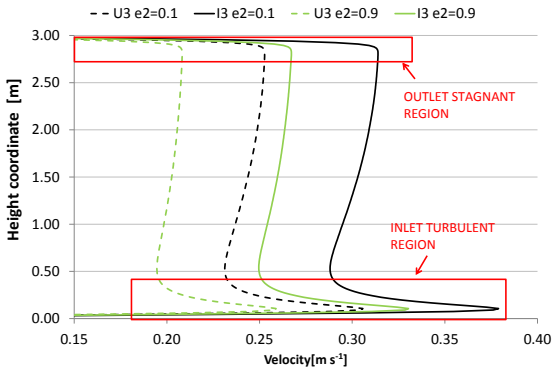

Fig. 7 – Velocity profiles for cases U3 and I3 close to the cavity inner surface.

4.2 Effect of outdoor air temperature

In addition to the cavity thickness and height and to the surface emissivity, also the influence of air temperature on the surface thermal resistance is investigated.

Figure 8 shows the trend of the surface thermal resistance as a function of temperature for the case studies already presented. In addition to this, the graph also shows the surface resistances computed by the method provided in annexe A of the standard EN ISO 6946. The latter considers the dependence of the temperature only in the radiative contribution, while the convective resistance is assumed to be constant.

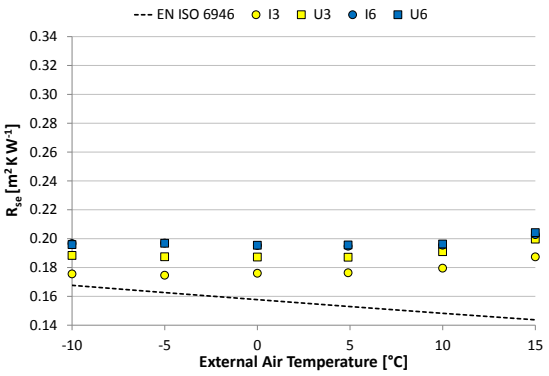

Fig. 8 – Surface resistance as a function of Te (d= 15 cm, e2 = 0.9)

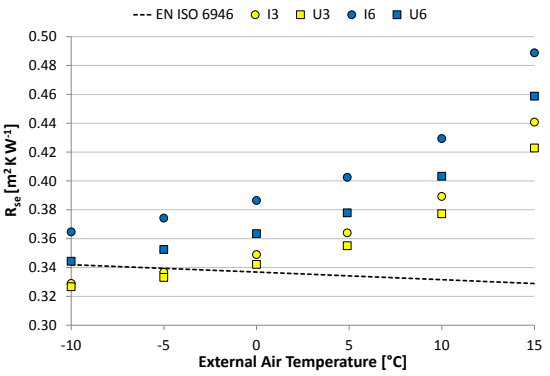

Fig. 9 – Surface resistance as a function of Te (d= 15 cm, e2 = 0.1)

The graph points out a slight underestimation of the resistance computed by means of the standard correlation. This obviously occurs because the convective resistance of the standard takes into account the unfavourable condition of motion caused by wind forces. In this case the higher air velocity in the channel greatly reduces the convective thermal resistance. However, it can be seen that the gap between EN ISO 6949 and thermo-fluid dynamic simulations increases for high external temperatures.

In fact, from the comparison among the data obtained from the thermo-fluid dynamic model a weak dependence of the total thermal resistance on the outdoor temperature emerges. This is probably linked to the compensation between the increase of the convective flow, tied to the higher air velocity, with the decrease of exchange by radiation.

Therefore the standard relation for the calculation of the radiative thermal resistance, obtained by linearizing the equation of the radiative heat exchange, describes in an opposite way the resistance trend linked to temperature variations. This emerges even more clearly if the behaviour of cavity with low emissivity surface is analysed (Figure 9).

Note that while the resistance calculated from the thermo-fluid dynamic analysis tends to increase with an increase in outside temperature, the EN ISO 6946 approach shows a downward trend.

4.3 Resistance data dispersion

Finally, the paper focuses on the analysis of the dispersion of the surface thermal resistances. Assuming the development of a relationship that binds the surface thermal resistance to some parameters such as surface emissivity and cavity thickness, the purpose is to investigate the data dispersion induced by other parameters. Therefore, the spreads in the values caused by the outside air temperature, by the height of the ventilation channel and by the insulation level of the wall behind the cavity are studied.

The simulation results are summarized in the box plot (Figure 10 and Figure 11) where the degree of dispersion and skewness in the distribution are fully described by means of the minimum, lower quartile, median, upper quartile and the maximum of observations.

The graph in Figure 10 shows the box plot obtained for several configurations using an emissivity of the inner surface of the cavity of 0.9. The box plot clearly shows a limited symmetrical dispersion of the data. Only when the thickness is equal to 6 cm, does the distribution assume a slightly asymmetric shape with an approach of the maximum value to the upper quartile. Besides, the difference between various thicknesses seems to be linked to a mere translation of the graph around another median value.

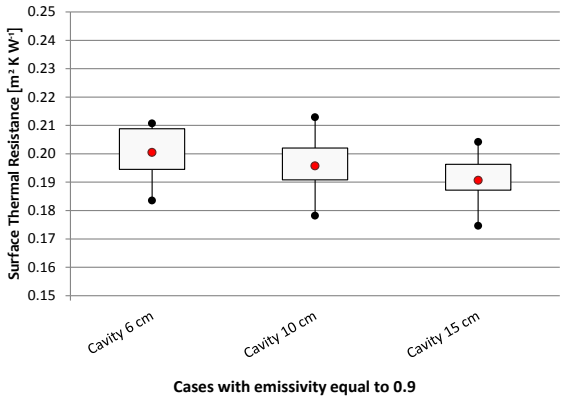

Fig. 10 – Variability of surface thermal resistance.

The distribution features change, however, if the resistance to irradiation increases due to reduced emissivity of the cavity inner surface (Figure 11). The graph indeed shows a high skewness of the distribution for all the thickness analysed. In particular, there is a greater distance between the maximum value and the upper quartile. This is mainly related to the high dependence of the radiative thermal resistance on the temperature. Since in low emissivity cases the ratio of radiative resistance over total thermal resistance increases, this dependency becomes more visible. Moreover, the chart in Figure 11 stresses again the limited dependence of the results variability on the cavity thickness. In fact, when the cavity thickness increases the box plot simply translates to a lower median resistance.

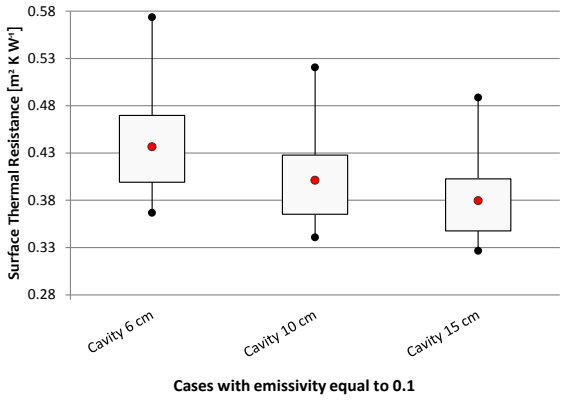

Fig. 11 – Variability of surface thermal resistance.

5. Conclusion

This paper has shown an analysis about the vented cavity behaviour under winter conditions. In particular the energy performances of several configurations are investigated by means of a coupled thermo-fluid dynamics model.

In addition to the cavity behaviour as a function of aspect ratio (e.g. thickness and length of the ventilation channel), the results stress a high dependence on the emissivity of the inner surface of the cavity. Results point out that, due to the higher surface temperature, when the emissivity decreases in insulated walls, the surface resistance increases much faster with respect to uninsulated cases. Therefore, these results highlight the effectiveness of reflective foil coupled with both traditional insulation and ventilation cavity.

Another result obtained regards the variability of the resistance to the boundary temperatures. While for normal emissivity (of the order of 0.9) the resistances show a poor temperature dependence, when the emissivity decreases the total thermal resistance is strictly connected to the boundary temperatures.

Thus, for these cases the simplified approach for the surface resistance calculation should be refined. In fact, an incorrect modelling of the thermal resistance trend caused by the outside temperature emerges from the comparison between the simplified approach of the standard EN ISO 6946 and enhanced calculation method. However, it should be stressed that in insulated walls the contribution of the ventilated cavity on the total thermal resistance is smoothed over by the insulating layers. Consequently, the dispersion of surface thermal resistance may have a limited effect on the energy demands.

In conclusion, this work has enabled us to deepen our understanding of the mechanisms of heat transfer in the ventilated cavity under steady state conditions. In future developments, this model can be applied to transient regimes in order to evaluate the behaviour under real external conditions.

6. Nomenclature

Symbols

F	Volume force vector [N m^{-3}]
H	Cavity height [m]
I	Identity tensor [-]
T	Temperature [K]
c_p	Specific heat [J kg^{-1} K^{-1}]
d	Cavity thickness [cm]
e_2	Emissivity of the internal surface of the ventilated channel [-]
f	Decrement factor [-]
g	Gravity acceleration constant [m s^{-2}]
k	Turbulent kinetic energy
$\hat{n}$	Surface normal versor [-]
p	Pressure [Pa]
s	Thickness [m]
t	time [s]
u	Vector of velocity [m s^{-1}]

Greek

ϕ	Specific heat flux [W m^{-2}]
ε	Turbulent kinetic energy dissipation rate [-]
η	Dynamic viscosity [Pa s]
λ	Thermal conductivity [W m^{-1} K^{-1}]
ρ	Specific mass [kg m^{-3}]

Subscripts/Superscripts

0	initial condition
i	internal side of the sample
e	external side of the sample
s	referred to surface quantities
T	referred to turbulent quantity

References

CEN 2008. EN ISO 6946:2008, Building components and building elements - Thermal resistance and thermal transmittance -Calculation method

Ciampi, M., Tuoni, G. 1998. Periodic heat flow through ventilated walls. La Termotecnica, 9, p. 79-87

Ciampi, M., Leccese, F., Tuoni, G. 2003. Ventilated facades energy performance in summer cooling of buildings. Solar Energy, 75, p. 491-502

Falk, J. Sandin, K., 2012. Ventilated rain screen cladding: Measurements of cavity air velocity estimation of air change rates and evaluation of driving forces. Building and Environment.

Gagliano, A., Patania, F., Nocera, F., Ferlito, A., Galesi, A. 2012. Thermal performance of ventilated roofs during summer period. Energy and Buildings, 49, p. 611-618

Gan, G., 2010. Simulation of buoyancy-driven natural ventilation of buildings—Impact of computational domain. Energy and Buildings, 42, p. 1290–1300

Hauke, G., 2002. A simple subgrid scale stabilized method for the advection-diffusion-reaction equation, Computer Methods in Applied Mechanics and Engineering, 191, p. 2925-2947

Nore, K. Blocken, B. Thue, J.V., 2010. On CFD simulation of wind-induced airflow in narrow ventilated façade cavities: Coupled and decoupled simulations and modeling limitations. Building and Environment, 45, p. 1834-1846

Pasut, W., De Carli, M., 2012. Evaluation of various CFD modeling strategies in prediction airflow and temperature in a naturally ventilated double skin facade. Applied thermal engineering, 37, p. 267-274

Susanti, L., Hommab, H. , Matsumoto, H. , Suzuki, Y. , Shimizu, M., 2008. A laboratory experiment on natural ventilation through a roof cavity for reduction of solar heat gain. Energy and Buildings, 40, p. 2196–220